View Article Online
DOI: 10.1039/D0MH01073A

ARTICLE

Highly Transparent Photochromic Films with Tunable and Fast Solution-like Response

Received 00th January 20xx,
Accepted 00th January 20xx

DOI: 10.1039/x0xx00000x

Héctor Torres-Pierna,[a,b] Daniel Ruiz-Molina,[b] Claudio Roscini[b,*]

The increasing interest towards photochromic films and their practical applications are driving researchers to the continuous design and synthesis of novel organic photochromic dyes with optimized performances in polymeric matrices. However, whereas their photochromic properties could be readily rationalized in organic liquid solutions, these could not be directly extrapolated to polymers as their performance changes unpredictably upon integration into a solid matrix. This leads to a time-consuming synthetic re-tuning of the dye chemical structure and/or the polymeric medium. To avoid this, herein we report an efficient, straightforward and universal strategy to embed commercial T-Type organic photochromic dyes of different nature in a polymeric material without compromising their optimum solution absorption and isomerization kinetics. Our approach is based on trapping emulsified nanodroplets of a hydrophobic solution enclosing the dye into a hydrophilic polymeric matrix. The material is prepared through one single process using commercially available materials, without further modification of the components (the dye and the polymer matrix) nor requiring previous encapsulation steps. The films, which manifest true solution liquid-like and finely tunable photochromic behavior, are also highly transparent, recyclable, scalable, and show enhanced fatigue resistance, making them highly suitable for different smart glass applications.

Introduction

The reversible light-induced color change of photochromic materials is of great interest for the fabrication of light-responsive devices, such as dynamic optical filters, rewritable displays, optical memories, smart biomaterials, etc.[1–10] Among the different possibilities, those materials based on organic photochromic dyes (mainly spirooxazine and naphthopyran derivatives)[7,11] are increasingly attracting the attention of the scientific and industrial sectors due to their broad commercial availability, relative good fatigue resistance and easy tunability of the optical properties.[12,13] Specifically, most relevant industrial applications are typically based on T-type organic photochromic dyes: under UV radiation, these dyes reversibly interconvert from a thermodynamically stable colorless closed form to a more energetic photoactivated colored merocyanine (MC)-like isomer, which reverts back to the initial ring-closed state in the dark through spontaneous thermal relaxation.[11] This photochromism allows to obtain self-responding photoprotective coatings, which use is currently limited to photochromatic ophthalmic lenses.[12,13]

In liquid solutions, the photochromic response (e.g. color type and intensity of the activated form, fading rate, etc.) can be easily correlated to the dye chemical structure, the solvent polarity and viscosity, allowing for straightforward and often predictable fine tuning of the optical properties.[14–16] Unfortunately, this does not apply to solid solutions, i.e. photochromic polymeric films, which are far more relevant for practical applications. In these, the photochromism is much more difficult to control, with kinetic responses dramatically slowed down or even inhibited.[6,13,17] This is due to the steric hindrance that the solid matrix opposes to the conformational changes of the photochromic molecules involved during the photoinduced and thermal back isomerization (also known as matrix effect).[14,18–20] This originates that the response of these dyes in commercial products, such as ophthalmic lenses, is far from being the best possible or prevents spreading out of these dyes to many other sectors.

To accomplish as much as possible matrix-independent photochromic responses, researchers have explored two main strategies over the years. The first approach consists in the synthesis of new photochromic molecules with minimal conformational changes along the photochromic interconversion to minimize the matrix effect. This has been mainly achieved with imidazole-based molecules,[21–33] prepared by Abe et al., or preventing the formation of the naphthopyrans (transoid-trans)[34–43]/spirooxazines (trans-merocyanines)[44,45] long-lived isomeric open form, responsible for the slowdown of the ring-closure reaction (oxazines, substituted

[a] Futurechromes S. L., Carrer Còrsega 516, 08025 Barcelona, Spain.
[b] Catalan Institute of Nanoscience and Nanotechnology (ICN2), CSIC and BIST, Campus UAB, Bellaterra, 08193 Barcelona, Spain.
E-mail: claudio.roscini@icn2.cat

Electronic Supplementary Information (ESI) available: [details of any supplementary information available should be included here]. See DOI: 10.1039/x0xx00000x

naphthopyrans). The second strategy is to facilitate the dye isomerization by providing softer (less steric hindrance) or void (free-volume) matrix environments. This has been accomplished by *i)* functionalizing the photochromic molecules with flexible tails,[46–50] *ii)* embedding the dyes in different media such as low glass transition and/or plasticized polymers,[51,52] hybrid organic/inorganic materials,[53–55] hydrogels,[56] or organogels,[57] and *iii)* encapsulating the molecules in the cages of hybrid mesostructured (nano)materials,[58–62] metal-organic frameworks,[63,64] and supramolecular assemblies.[65–67] The encapsulation was also explored by our group, which reported tunable photochromic properties (fast or reverse photochromism) in solid materials by embedding core-shell capsules into polymeric films,[20,68,69] a strategy that was also successfully extended to the fabrication of liquid-like thermochromic[70] and white-emitting[71] materials. However, despite all these advances, the implementation of these materials in commercial goods still faces real challenges as most of them are: i) too specific requiring determined cage dimensions, capsules with suitably designed shell material, plasticizers and/or chemically modified environments;[18,72] ii) difficult to scale up, as multiple steps and time-consuming synthetic procedures are required for the dyes functionalization, micro/nanocontainers fabrication and/or the film formation; and more importantly iii) opaque, since many of these approaches lead to non-optically transparent films. Therefore, there is still an urgent need to develop photochromic solid films that can be easily handled and incorporated in commercial products that require tunable photochromic responses and high transparency.

To overcome these important issues that are limiting the broadening of solid photochromic materials to various applications herein we designed and developed a novel strategy based on a polymeric matrix entrapping oil nanodroplets, which contain the photochromic dye. Whereas the continuous polymer matrix provides the mechanical properties to the material, the hydrophobic droplets constitute the soft medium that allows the dye molecules to interconvert as fast as in a liquid solution. Similar materials design has been successfully used to yield functional coatings and films of relevance in commercial electronic papers,[73] photoprotective packaging,[74] liquid crystal displays for smart windows,[75] or scratch-and-sniff coatings,[76] inter alia, obtained by trapping microdroplets of different materials in polymer matrices. However, in our case, the droplet size has to be reduced up to the nanoscale to minimize the light scattering and guarantee the high transparency of the film, which is a key requirement in smart glasses.[77]

The advantages of this strategy are remarkable. It represents a straightforward and universal solution for the preparation of highly transparent solid films with tunable and fast liquid solution-like photochromic response. Films can be prepared in one-pot step through a reaction-free and scalable processes, using readily available starting materials. On top of that, the photochromic performance can be fine-tuned by selecting the initial components of the mixture, without requiring chemical functionalization or modification neither of the photochromes nor the embedding matrix.

Results and discussion

Proof of concept of transparent fast-responsive photochromic films

A graphic representation of the experimental approach followed for the preparation of the films is shown in **Scheme 1**.

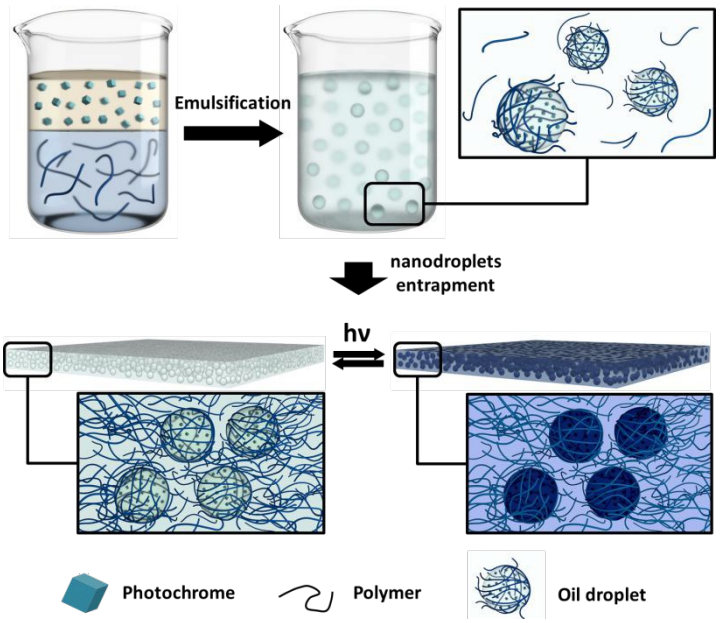

Scheme 1. Nanoemulsification and nanodroplets entrapment: schematic representation of (top) the o/w nanoemulsion formation and (bottom) nanodroplets entrapment (nanoemulsion entrapment) in photochromic films upon casting the emulsion on a surface and solvent evaporation. A schematic representation of the oil nanodroplets containing the photochrome molecules within the polymeric matrix is shown in the zoomed areas.

View Article Online
DOI: 10.1039/D0MH01073A

ARTICLE

First, an oil-in-water (o/w) nanoemulsion of hydrophobic nanodroplets (< 100 nm) containing the photochromic dye is obtained in the presence of a hydrophilic polymer that acts as both droplet stabilizer and film-forming material. Afterwards, the formation of the nanostructured film takes place upon water evaporation, resulting in the physical trapping of the photochromic nanodroplets within the matrix as a separated phase without droplet coalescence, which guarantees the formation of a highly transparent film.

For the first proof-of-concept the following three components were selected: as the dye we used the commercially available T-type spirooxazine 1,3-dihydro-1,3,3-trimethylspiro[2H-indole-2,3'-[3H]naphth[2,1-b][1,4]oxazine] (also known as Photorome I, PhI, see Supporting Information). In solution and under UV irradiation, PhI photoisomerizes from the spiro (SP) colorless form (λ_{max} = 322 nm in toluene) to the blue-colored MC-like isomer (λ_{max} = 593 nm in toluene), while fades completely in less than 10 s back to the colorless isomer in the dark (Scheme S1).[20] The oil of choice was Miglyol® 812 (M812), a coconut oil derivative (triglicerydes of capric/caprylic acids) that is colorless (to prevent color distortions of the photoactivated state), lipophilic (to permit the o/w emulsification and good separation from a hydrophilic polymer), of high boiling point (to guarantee long term stability of the film) and dissolves PhI without compromising its fast optical response.[20] Finally, a water solution of polyvinyl alcohol (PVA 4-88, i.e. low hydrolysis degree, low molecular weights) was used as aqueous phase. PVA is a good o/w emulsion stabilizer and has film-forming properties, both characteristics required for the formation of the polymer matrix entrapping the emulsified oil nanodroplets. It also exhibits high transparency in the visible and lowest-energy UV spectral regions, avoiding any interference with the photochromism of the dyes. Finally, PVA is well-known to have a low intrinsic oxygen permeability,[78,79] which should improve the dye fatigue resistance under irradiation (vide infra).

After mixing the aqueous PVA solution (20 wt.%) with the dye-containing oil mixture, ultrasounds (US) were used to obtain the o/w nanoemulsion (see Supporting Information for more details). The opacity of the emulsion gradually decreases with time, reaching a significant transparency after 20 min and a bluish coloration distinctive of the Tyndall effect (Figure 1a), produced by the dispersed nanodroplets that only scatter the shortest wavelengths (blue frequencies) of the incident visible light.[80] This qualitative observation was corroborated by dynamic light scattering (DLS) analysis, which showed an asymptotic decrease of the average droplets diameter down to approximately 90 nm with time (**Figure 1b** and S1). Finally, casting of the resulting o/w nanoemulsion onto a polystyrene Petri plate and posterior evaporation of the water gave a flexible and transparent free-standing **PhI@M812@PVA** film of ~ 150 μm thickness (**Figures 1c-d**). SEM analysis of a cross section of a cryo-fractured film showed the presence of porous structure (**Figure 1d**). Worth to mention, similar nanoemulsion entrapment films were obtained using the higher molecular weight PVA 40-88 (**PhI@M812@PVA-40**), in which holes (of diameter 50-200 nm), that correspond to the cavities left over by the oil droplets, can be differentiated (Figures S2a-b). Contrariwise, nanodroplets-free plain PVA 4-88 and PVA 40-88 films did not show these nanocavities, neither when the initial water solution was subjected to sonication, which might be argued to produce air nanobubbles (Figure S2c).

Differential scanning calorimetry (DSC) of the **PhI@M812@PVA** films (Figure S3a) showed an exothermic peak at -31 °C, associated to the solidification of M812 oil,[81] and a glass transition at T_g = 71.6 °C, only a few degrees lower than that of the plain PVA 4-88 film (T_g = 73.6 °C) studied under the same experimental conditions (Figure S3b). A further increase of the temperature also showed heat-flow variations in the range 140 °C and 200 °C, related to the melting of the PVA.[82]

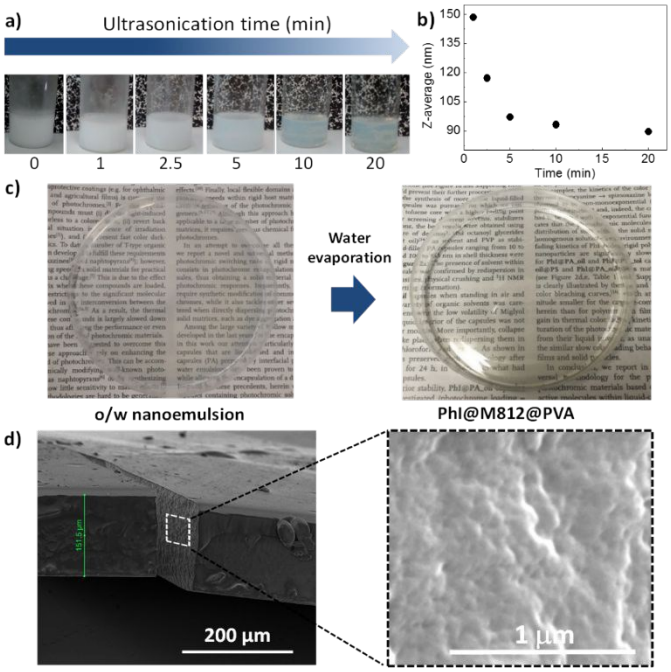

Figure 1. Nanoemulsion and photochromic film: a) images of a vial containing the o/w nanoemulsion at different sonication times; b) Z-average size for each one of the sonication times; c) image of the o/w nanoemulsion deposited on a Petri plate (left image) and of the resulting film obtained after the water evaporation (right); d) cross-section SEM image of the resulting **PhI@M812@PVA** self-standing film and a zoom of the section showing the porous structure.

The comparable oil solidification and the specific PVA transition temperatures found for the film and the isolated components, together with the SEM image shown in **Figure 1d**, seem to confirm that the polymer matrix and the oil nanodroplets remain mostly as two separated phases.

Thermogravimetric analysis (TGA) of both plain PVA and **PhI@M812@PVA** films showed the presence of ~ 6 wt.% of water (mostly removed before reaching 200 ºC), that possibly remained trapped during the film formation due to the hygroscopic character of the PVA (also confirmed by the DSC exothermic peak at around 0 ºC, Figure S3a), and thermal degradation of the film components only above 350 ºC (Figure S3c).

In the absence of irradiation, the colorless **PhI@M812@PVA** film exhibits high transmittance values in the high energy visible spectral range ($\%T^{400\text{-}450\ nm}$ ~ 89% respect to air reference and comparable to PVA plain films, Figures S4a-S4b). This indicates that the trapped nanodroplets are small enough to induce only a negligible light scattering, even for higher frequencies. In the dark, only an absorption band around λ_{max} = 319 nm, typical of the PhI spiro form can be found (Figure S4c). Upon UV irradiation (λ_{exc} = 365 nm), the film interconverts very fast (within a few seconds) to blue, associated to the appearance of the absorption band at λ_{max} = 603 nm ($\Delta Abs^{\lambda max}$ = 0.06), characteristic of the open MC form (**Figures 2a** and S4c).

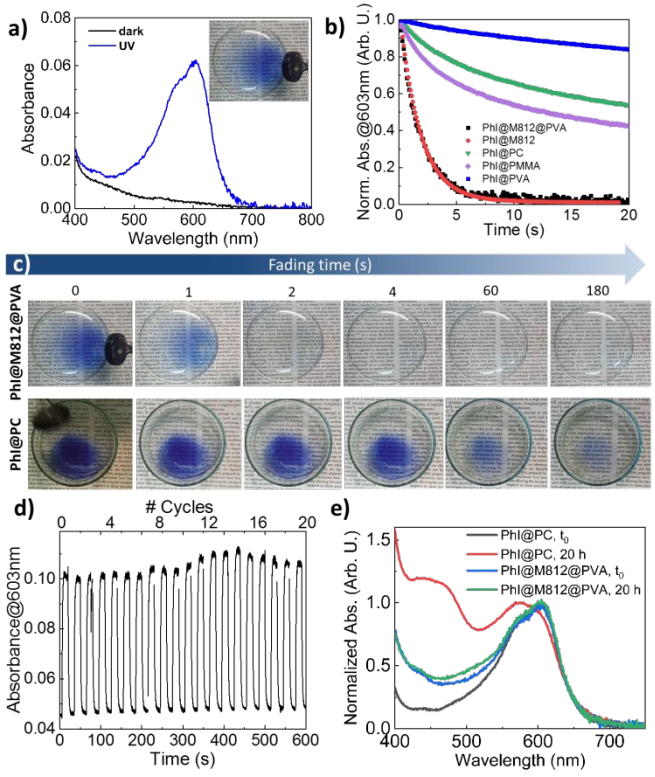

Figure 2. Photochromic performances of the films: a) absorption spectra of the **PhI@M812@PVA** film before and after UV irradiation and image of a film being irradiated (inset); b) fading kinetics of **PhI@M812@PVA**, **PhI@PMMA**, **PhI@PC**, **PhI@PVA** films and **PhI@M812** liquid solution, after reaching the photostationary state; c) snapshots of the fading of **PhI@M812@PVA** and **PhI@PC** films at different periods of time as indicated in the figure, where the difference in the discoloration kinetics between both samples is clearly reflected; d) coloration/fading cycles of **PhI@M812@PVA** film; e) absorption variation of the photoactivated **PhI@M812@PVA** and **PhI@PC** films, before and after 20 h of continuous irradiation with UV (365 nm, 2.5 mW cm^{-2}).

Interestingly, the normalized spectra of the photoinduced PhI open form in the film matches quite well with the one in a bulk M812 solution ($\lambda_{max}^{PhI@M812}$ = 601 nm, Figure S5). This underscores two important facts. First, the methodology used for the film preparation preserves the integrity of the dye. Secondly, the lack of a significant solvatochromic spectral shift of the PhI@M812@PVA ($\lambda_{max}^{PhI@M812@PVA}$ = 603 nm) film respect to the initial M812 solution of PhI ($\lambda_{max}^{PhI@M812}$ = 601 nm), indicates that there is a negligible diffusion/mixing of the dye and/or M812 to the hydrophilic PVA matrix along the film formation.

To investigate the discoloration kinetics in the dark, time-resolved UV-vis measurements were carried out at room temperature and at the absorption maximum of the MC isomer (λ_{max}^{MC} = 603 nm) after reaching very quickly the photostationary state (< 5 s, Figure S6a). The film spontaneously discolored through a first-order monoexponential decay function ($k^{PhI@M812@PVA}$ = 0.56 s-1, R2 = 0.995) with characteristic fading kinetics of homogeneous liquid solutions ($k^{PhI@M812}$ = 0.56 s^{-1}, **Figures 2b** and S6b-c). The matching of normalized fading kinetics of the **PhI@M812@PVA** film and of the bulk M812 solution, provides a further evidence of the negligible diffusion of the dye from the oil phase to the PVA matrix. The film recovered the colorless state in less than 10 seconds (Figure 2c and the Video S1) and the measured half ($t_{1/2}$) and three-quarters ($t_{3/4}$) fading times were just 1.4 and 2.7 s, respectively.

Reproducible photochromic properties were obtained when nanoemulsion-based films were prepared with other hydrophilic matrices of different molecular weight (i.e. PVA 40-88) or nature (i.e. hydroxylethyl cellulose, HEC) respect to PVA 4-88 polymer. Remarkably, both **PhI@M812@PVA-40** and **PhI@M812@HEC** films showed the same photoactivated species (λ_{max} ~ 600 nm, Figures S7a-b) as **PhI@M812@PVA** and, most importantly, very fast fading responses ($t_{3/4}^{PhI@M812@PVA\text{-}40}$ = 2.1 s; $t_{3/4}^{PhI@M812@HEC}$ = 3.1 s, Figure 7c), indicating that this strategy guarantees the photochromic dye to remain dissolved in the oil phase and, thus, the liquid-like response of the film. However, PVA-based films (i.e **PhI@M812@PVA** and **PhI@M812@PVA-40**) were much more transparent than that **PhI@M812@HEC** film, which suggests that PVA, regardless the molecular weight, is a more suitable polymer for the stabilization of the oil nanodroplets during the nanoemulsion formation and/or the film drying and minimize the scattering associated to the oil-droplets. Homogenous PVA-based polymer-dispersed photochromic organogels had been reported in the past,[57] but the combination with such a fast liquid solution-like discoloration process and high transparency (%T ~ 90%, in the non-activated state) is unprecedented.

For comparison purposes, a nanoemulsion-free film was prepared by directly dispersing PhI dye in the PVA matrix. Due to the low solubility of the dye in the hydrophilic polymer, the obtained **PhI@PVA** film was slightly opaque and presented higher scattering at shorter wavelengths (Figure S8). More transparent photochromic films of poly(methyl methacrylate)

(PMMA) and poly(bisphenol A carbonate) (PC), of relevance for several applications, were prepared by directly embedding the dye in these polymers. Despite the photochromic response in these films was preserved (Figure S9), decay studies showed that the fading kinetics of PhI are one or two orders of magnitude slower ($t_{3/4}^{PVA}$ = 349 s, $t_{3/4}^{PMMA}$ = 65 s, $t_{3/4}^{PC}$ = 127 s) than that observed for **PhI@M812@PVA** film (**Figures 2b-c**, S6b-c, S8, Video S1, and Table S1). Moreover, these **PhI@PMMA PhI@PC** and **PhI@PVA** films faded following multiexponential decay functions due to the matrix inhomogeneity and the presence of distinct microenvironments created by the polymer around the embedded dyes.

Finally, the radiation-induced coloration and spontaneous fading cycle of the **PhI@M812@PVA** film was repeated at least for 20 times in a row without any detectable dye degradation (**Figure 2d**). Additional fatigue resistance experiments of the film by continuous irradiation for 20 h at λ_{exc} = 365 nm showed no significant variation of the photoactivated states, whereas remarkable changes were detected in a **PhI@PC** film under the same experimental conditions (**Figures 2e** and S10). Such good fatigue resistance showed by the photochrome in the **PhI@M812@PVA** film, even in the absence of additional stabilizers (e. g. UV absorbers, oxygen and radical scavengers),[83] was correlated to the inertness of the dissolving oil and to the intrinsic high impermeability of PVA to oxygen,[78,79] which is known to be one of the causes of the photochromic materials degradation.[11,84,85]

Tuning of the spectral and fading kinetics properties.

The versatility and flexibility of our approach was demonstrated by developing novel **dye@solvent@PVA** films where the dye and the oil used for the emulsification have been systematically tuned to control the optical response of the films.

Dye modification. For these experiments, M812 was maintained as the oil of choice for the nanodroplets, while different commercially available spirooxazines and naphthopyrans dyes of distinct colors in their photoactivated state, were used. Some of the resulting **dye@M812@PVA** films presented a residual color related to the intrinsic low absorption properties of the dye in its dark state. All films colored (or enhanced their coloration) upon irradiation with a UV radiation source (λ_{exc} = 365 nm, 2.7 mW/cm^2), solar simulator (~ 0.44 W/m^2) or ambient sunlight. Films obtained from the spirooxazines Palatinate Purple (PP),[86] Aqua Green (AG), Claret (CL) or naphthopyrans Berry Red (BR)[14] and Rush Yellow (RY)[12] displayed the instantaneous appearance of well-defined absorption bands with λ_{max} covering different visible spectral regions, and therefore different colors (**Figures 3a-b** and S11). Those obtained from Misty Grey (Misty), Midnight Grey (MD) and Graphite (GR) yielded neutral grey colors with broad absorptions in the whole visible spectral region (**Figures 3a** and **3c**)‡ Finally, neutral color was also achieved by entrapping a mixture of complementary colored dyes in their photoactivated state, such as AG and BR (**Figures 3c** and S12).

All these films developed intense coloration under ambient solar irradiation ($\Delta Abs^{\lambda max}$ = 0.3 – 1), reproducing the spectral features and $t_{1/2}$ and $t_{3/4}$ fading times (in the dark) of the dye in a M812 solution (Figures S13-S14,Table S2). The discrepancies of $t_{1/2}$ and $t_{3/4}$ fading times of the M812 solutions and the **dye@M812@PVA** films observed for some dyes were ascribed to temperature variations during the measurements and/or to interactions (e.g. hydrogen-bonding interaction) that these could establish with the matrix at the oil/PVA interface. Nevertheless, in all cases these films discolored much faster than the corresponding **dye@PMMA** films (which show comparable spectral features, Figures S11 and S13), reaching fading times up to two orders of magnitude shorter (Figures S14-S15, Videos S2-S3, Table S2). Actually, based on the intrinsic response of the dyes in M812 ($t_{1/2}$ and $t_{3/4}$ values), it is possible to make the following dye classification: very fast (PhI, Misty, PP), medium (AG, CL, RY, MD) and slow (BR, GR), which is preserved in the **dye@M812@PVA** films. This order cannot be extrapolated for the PMMA films prepared with the same dyes. This is due to fact that the media in which the dyes are embedded are different, being i.e. the M812 oil for the solution and the **dye@M812@PVA** film and a rigid matrix for the PMMA film. Moreover, the matrix effect given by the rigid PMMA matrix and the hindering caused by the polymeric chains on the embedded dyes, make the photochromic response much more dependent on the volume changes involved in the interconversion, compared to what happens in the liquid oil (Table S3). These results suggest that the nanoemulsion entrapment technique is a valid approach to produce transparent photochromic films with liquid-like and predictable behavior (based on data in liquid solution) with any commercial or newly synthesized T-Type photochromic dyes, provided these are soluble in the oil medium.

Oil modification. Given the solvatochromism and the ring-closure rate dependency of the open form of these dyes with the solvent polarity and viscosity,[15,87,88] the oil of choice is also expected to confer an easy way to fine tune the photochromic properties of the films. To explore this possibility, the commercially available PP spironaphthoxazine was dissolved in various high boiling point oils of different polarity and viscosity (see Table S4 for the full list). When the nanoemulsion entrapment process was carried out with these solutions highly transparent **PP@oil@PVA** films with $\%T^{500nm}$ > 85%§ were obtained, except for the 3-phenyl bicyclohexyl (3PhbCH) and hexylbenzene (HxBz) oils that provided opaque films (Figure S16, Table S4). Upon UV irradiation, all films turned blue (Figures S17) with shifts in the absorption maxima (λ_{max}) up to 18 nm between different oils (Figure S18a and Table S4). Even more dramatic was the difference in the fading kinetics with $t_{1/2}$ and $t_{3/4}$ values that varied up to 7 times (**Figures 3d** and Table S4). Moreover, it was found a relationship between λ_{max} and $t_{1/2}/t_{3/4}$ values: **PP@oil@PVA** films absorbing at longer wavelengths (in the photoinduced state) were also the ones with the shortest $t_{1/2}$ and $t_{3/4}$ values (fastest to fade), and vice versa (**Figures 3e** and S18b).

View Article Online
DOI: 10.1039/D0MH01073A

ARTICLE

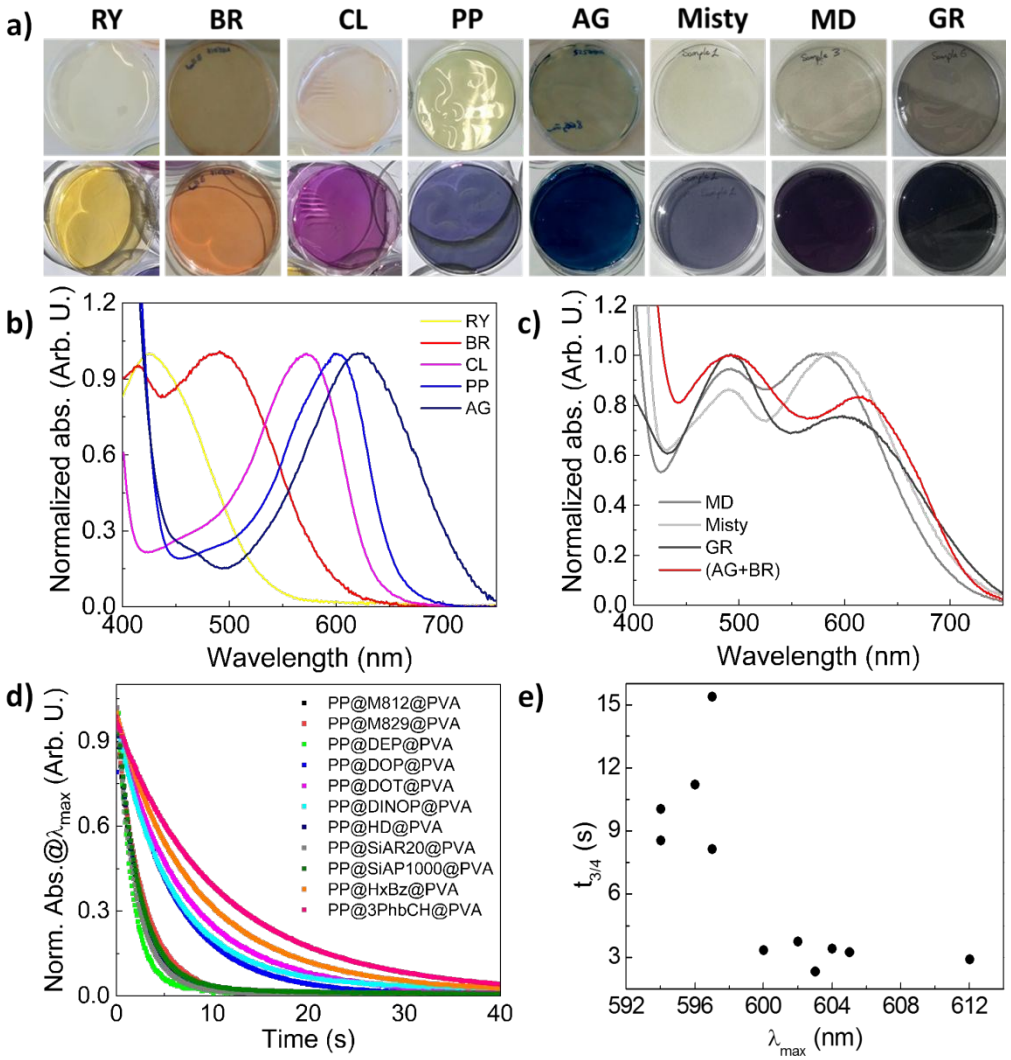

Figure 3. Tunability of the films photochromic response: a) **dye@M812@PVA** films both in the dark (upper figures) and their photoinduced color state under ambient sunlight irradiation (bottom figures); b-c) absorption spectra of **dye@M812@PVA** films in their photoinduced color state; d) fading kinetics and e) trend of $t_{3/4}$ vs λ_{max} of photoinduced colored **PP@oil@PVA** films. Dye names abbreviations: RY, rush yellow; BR, berry red; CL, claret; PP, palatinate purple; AG, aqua green; Misty, misty grey; MD, midnight grey; GR, graphite. Oil names abbreviations: M812, Miglyol® 812; M829, Miglyol® 829; DEP, diethyl phthalate; DOP, dioctly phthalate; DOT, dioctyl terephthalate; DINOP, diisononyl phthalate; SiAR20 and SiAP1000, silicon polyphenyl-methylsiloxane oils (~ 20 mPa.s and ~ 1000 mPa.s, respectively); HD, hexadecane; HxBz, hexylbenzene; 3PhbCH, 3-phenyl-1,1'-bicyclohexyl.

This type of correlation is typically reported for liquid solutions of T-Types photochromic dyes.[14,15,87,88] These results reveal that by using a fixed dye, a fine tuning of the photochromic properties is accomplished by simply varying the oil component of the film, without requiring the modification of the matrix rigidity or the use of plasticizers.

As expected, the photochromic properties resulted to be independent on the matrix used: the absorption spectrum and the fading rate of the film prepared from a M812 solution of PP and PVA 40-88 matrix material (**PP@M812@PVA-40**) overlap with those of **PP@M812@PVA** (Figure S19).

Large area films and derived prototypes

After demonstrating the viability and the versatility of the nanoemulsion entrapment method for the achievement of fast-responsive and tunable photochromic films, we aimed to use them to prepare product prototypes. This involved two steps: first the fabrication of photochromic films with suitably large dimensions and second their implementation in the prototypes.

Large area films. Before fabricating films large enough for the prototypes, it was necessary to scale up the preparation of the nanoemulsions obtained by sonication (~ 10 g). For this we used a high-pressure-homogenization equipment, where up to

View Article Online
DOI: 10.1039/D0MH01077A

250 g of the mixture is reprocessed several times yielding a nanoemulsion with similar droplets size distribution as for that obtained through ultrasonication (Figure S20). Thanks to the nanoemulsions kinetic stability,[85] the resulting mixture turned out to be stable for several months. This long-term stability allowed to obtain films with fairly reproducible transparency ($\%T^{450nm}$ > 85%, Figure S21) from nanoemulsions stored for up to three months at room temperature.

The nanoemulsion mixture resulting from each batch is enough as to allow for the fabrication of at least 30 identical 8.5 cm diameter photochromic films (~ 64 cm2), as those shown in Figure 3. The same volume can be used to prepare films of much larger surface areas (up to 22 X 40 cm^2) and similar transparencies ($\%T^{450nm}$ ~ 85%) through casting or a Dr. Blade applicator (Figure S22).

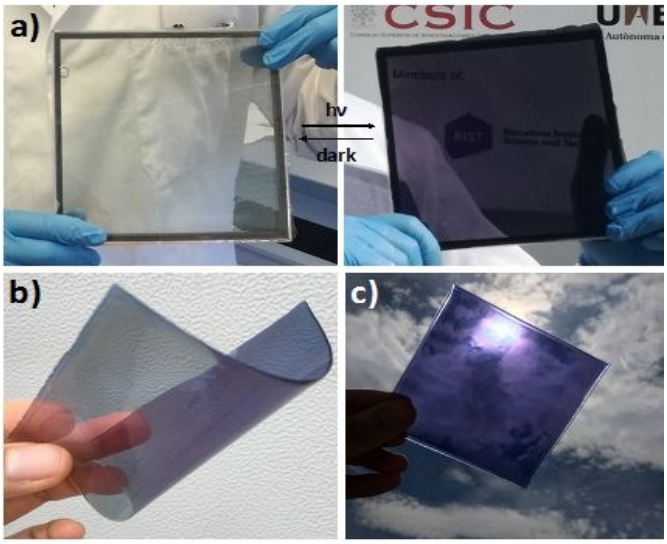

Figure 4. Scaled up coatings or self-standing films: images of a) glass coated with a **GR@M812@PVA** film prepared through nanoemulsion entrapment process, in the dark and under ambient sunlight irradiation, b) pealed out flexible 15x15 cm^2 **CL@M812@PVA** photochromic film and c) the laminated photochromic glass using the **CL@M812@PVA** film, under ambient sunlight irradiation.

These large area films (90-200 μm in thickness) retain the characteristic photochromic properties and can be fabricated as coating, directly adhered to the substrate (**Figure 4a**) or pealed out yielding flexible and self-standing films (Figure 4b) that could be used in laminates between glasses (**Figure 4c**) or other substrates.

Moreover, these films revealed to be completely recyclable. Indeed, given the water solubility of PVA, the film (e.g. **Misty@M812@PVA** film) could be re-dissolved in warm water, upon stirring, and reformed several times, through casting. The recycling process could be successfully carried out with or without introducing the homogenization step (e.g. sonication) before the re-casting on the Petri plate. In each case it was possible to re-obtain, after the first and the second recycle, quite transparent films, reproducible spectral properties ($\%T^{450nm,\ dark}$ ~ 80%; $\%T^{450nm,\ UV}$ ~ 63%) and fading response ($t_{1/2}$ ~ 3 s and $t_{3/4}$ ~ 8 s, Figures S23-S24).

Prototypes. Finally, we aimed to prepare various prototypes of products where transparent photochromic materials of different responses are required. Some of the applications where these new films are expected to have a great impact are photochromic glasses, helmet face shield and antiglare mirrors, where both transparency and fast fading response are key features. For the fabrication of photochromic sunglasses (**Figure 5a**), the **dye@M812@PVA** films, prepared with the fast fading PP or Misty dyes, were layered between two curved glasses, which were then cut with the appropriate dimension and shape (see supporting information for more details). For the helmet face shield (**Figure 5b**), a neutral **grey@M812@PVA** film was prepared using the Dr. Blade applicator and adhered in the internal surface of the face shield. The mirror was coated with a neutral **grey@M812@PVA** film (**Figure 5c**), prepared by direct casting the nanoemulsion on the top surface, and letting the water evaporate. The photochromic glasses and the helmet face shield colored under UV sources or solar light radiation and maintained the liquid solution-like fast photochromic response, recovering the initial state, in the dark, in less than 1 min.

Noticeably, despite the films for non-flat photochromic glasses required to be thermoconformed, at 60 °C for 1 min, to provide the curved shape of the lenses, the final prototypes retained quite well the optical transparency (%T > 80%), the spectral properties ($\lambda_{max}^{PP@M812@PVA}$ = 600 nm; $\lambda_{max}^{Misty@M812@PVA}$ = 489 and 588 nm) and the fast fading response ($t_{3/4}^{PP@M812@PVA}$ = 4.0 s, $t_{3/4}^{Misty@M812@PVA}$ = 7.5 s) of the initial films (Figure S25, Videos S4). The mirror reduced the reflectance of visible light from 92% to 56% upon exposition to sunlight (Figure S26), suggesting a potential applicability for vehicle external rear-mirrors.

Finally, the prototype of a rewritable device (**Figure 5d**), of interest for commercial applications, was also obtained by laminating a **PP@M812@PVA** film between two glasses. Upon irradiation of the device with a 405 nm laser pointer or a phone torch light (PP has residual absorption in the visible region) it is possible to produce instant and high contrast handwritings or drawings, which very quickly erase once the irradiation is stopped (Video S5).

Another area of potential relevance for these photochromic films is construction. Windows glasses coated with smart optical filters that guarantee a dynamic filtering of the visible light during very sunny days, are of interest in the building industry for improving comfort and reducing the amount of heat entering in the building. Smart windows prototypes were prepared by layering the **dye@M812@PVA** films between glasses and installing the laminates in a house model. The windows colored under sunlight and recovered their colorless state in the dark (**Figure 6a**). To investigate their effectiveness in contrasting the heat increase during sunlight exposition, photochromic windows were prepared by coating the glasses with the **GR@M812@PVA** film, through casting method and letting the water to evaporate. The same film was applied onto a standard glass slide and a commercial low-emitting insulating glass unit (low-E IGU, **Figure 6b** and S27a), generally used to increase the energy saving in buildings. A solar simulator (1 W/m^2) was used to irradiate for 30 min, a holed cardboard box through the coated photochromic glasses (simulating a window), layered on top of the hole (see Supporting Information for more details).

View Article Online
DOI: 10.1039/D0MH01073A

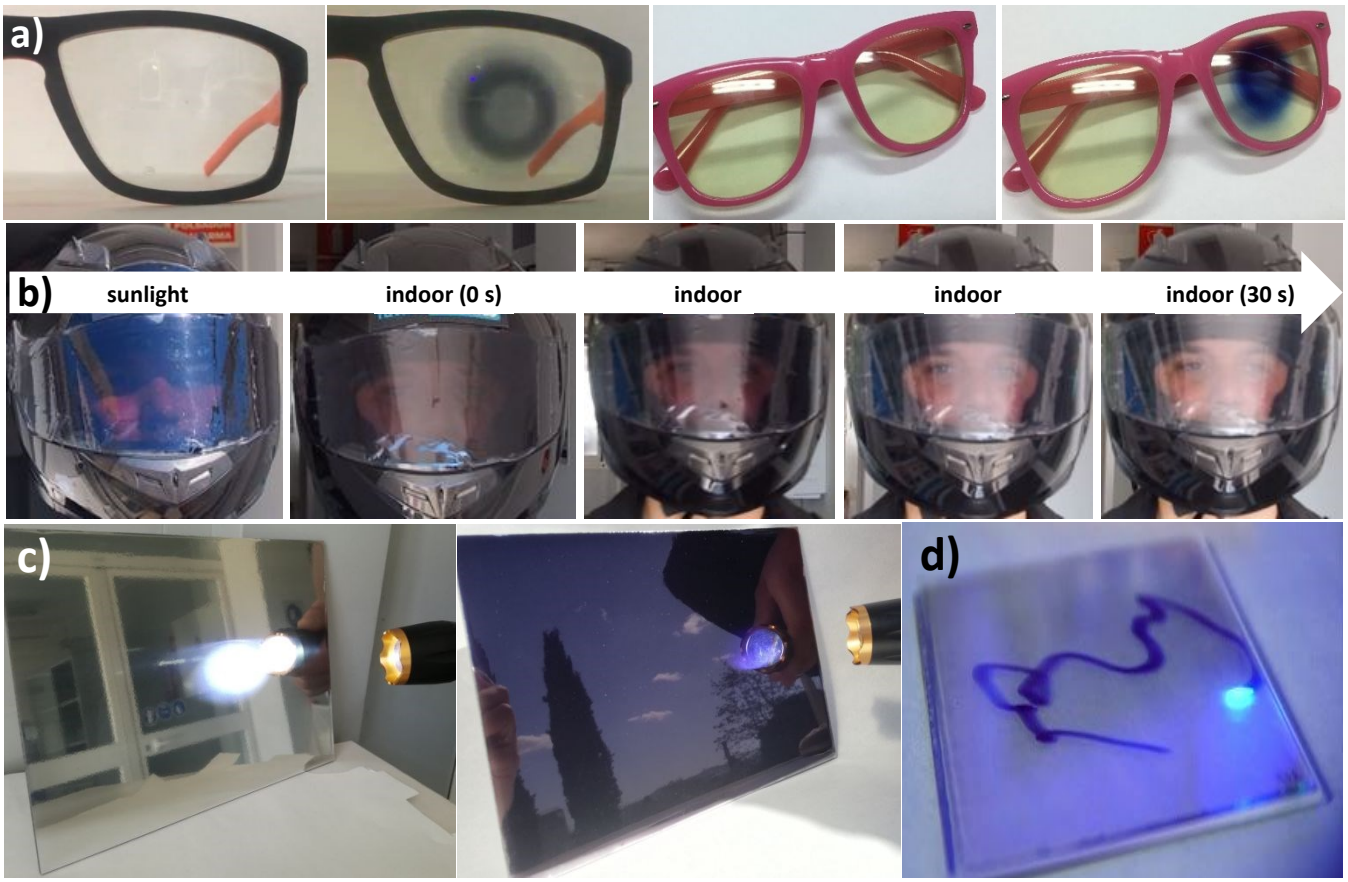

Figure 5. Prototypes with fast fading response: a) two different sets of glasses obtained from thermoconformed photochromic **dye@M812@PVA** films, showing coloration under irradiation; b) fast discoloration kinetics (< 30 s) of a helmet face shield coated with our film; c) mirror coated with the **dye@M812@PVA**, film evidencing the different reflectance of visible light, in the dark and under UV irradiation or solar light; d) snapshot of the handwriting on the rewritable device prototype.

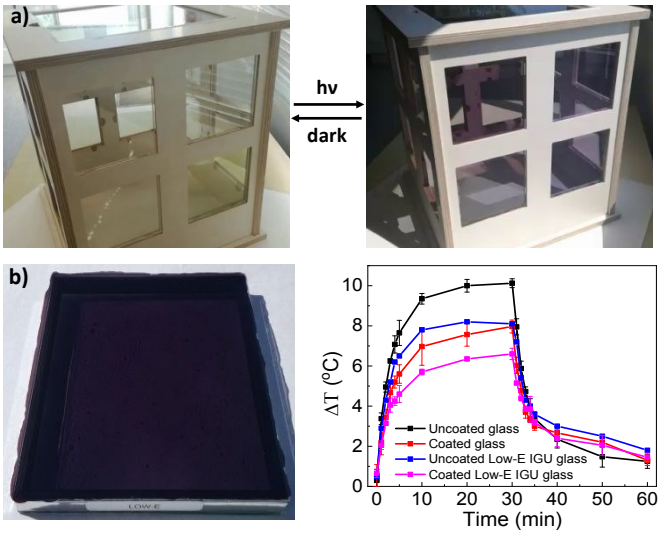

Figure 6. Prototypes for smart windows application: a) house model containing laminated windows prepared with different **dye@M812@PVA** photochromic films, in the dark and under ambient solar irradiation; b) low-E IGU glass coated with **GR@M812@PVA** film under sunlight irradiation and temperature increment (ΔT) caused by solar simulator irradiation (1 W/m²) through glasses coated or not with the **GR@M812@PVA** film.

The inside temperature increase, respect to the outside constant room temperature, was monitored with a thermometer (Figure S27). Irradiations through uncoated glasses were also carried out as control experiments. Interestingly, when the coated standard glass was used as window, it darkened and the temperature increment (ΔT) inside the box upon irradiation reduced from 10 to 8 °C, respect to the same window without the photochromic film. The temperature increment was further reduced (to only 6.5 °C) when a low-E IGU glass coated with **GR@M812@PVA** film was used (the uncoated low-E IGU reduced the ΔT to 8 °C), suggesting that these films could be also adapted to energy-saving applications (**Figure 6b**).

Conclusions

A novel simple, one-pot and reaction-free protocol, using readily available materials, has been shown effective for the fabrication of photochromic films with liquid solution-like response. This disruptive, but easy methodology, relies on the entrapment of oil nanodroplets containing the photochromic dye within a polymer, without additional chemical modifications nor the use of plasticizers. This approach overcomes most of the challenges that are preventing

photochromic materials to be used in different applications and that were only partially solved by the several previously developed strategies. The resulting films exhibit high optical transparency, fast fading kinetics, enhanced fatigue resistance and good colorability. Moreover, the photochromic response of the final films can be systematically fine-tuned by changing the dye and/or the oil of the droplets. Compared to previously reported core-shell capsules strategies, the nanoemulsion entrapment approach also prescinds of the shell material, allowing the embedment of a larger volume of the dye solution. This approach is extendable to whichever T-Type (and also P-Type) organic photochromic dye soluble in the oil medium.

Thanks to this ground breaking material, we were able to obtain photochromic prototypes of relevance not only for glasses with enhanced performances but also for other commercial areas such as helmets, mirrors, rewritable displays or smart windows, with promising energy-saving properties. Worth to emphasise is also that i) the films can be implemented through different approaches, from in-situ coatings to flat/curved laminates from the pre-formed self-standing flexible films; ii) the film could be re-dissolved and recycled as novel film or coating, reducing waste and increasing the life-cycle of the material, iii) the nanoemulsions are storable for several weeks, and iv) both nanoemulsion and film preparation are fully scalable. All in all, these results evidence this approach is very promising for applications requiring fast and easily tunable photochromic responses.

Conflicts of interest

There are no conflicts to declare.

Acknowledgements

This work was supported by grants from the Spanish Research Agency funds (AEI, grant no. RTI2018-098027-B-C21) and by the European Regional Development Fund (ERDF). The ICN2 is funded by the CERCA programme / Generalitat de Catalunya. The ICN2 is supported by the Severo Ochoa Centres of Excellence programme, funded by the Spanish Research Agency (AEI, grant no. SEV-2017-0706). H. T. P. thanks the Generalitat de Catalunya (AGAUR) for the fellowship Doctorats Industrials. The authors acknowledge Futurechromes S. L. for the funding.

Notes and references

‡ The mentioned dyes are commercially available, though their chemical structures are not disclosed in most of the cases.

§ $\%T^{500nm}$ was chosen for these films to avoid the absorption contribution of the dye, in the dark, in the high-energy visible region.

1 M. Irie, *Chem. Rev.*, 2000, **100**, 1683–1684.
2 G. Berkovic, V. Krongauz and V. Weiss, *Chem. Rev.*, 2000, **100**, 1741–1754.
3 J. Zhang, Q. Zou and H. Tian, *Adv. Mater.*, 2013, **25**, 378–399.
4 J. Zhang, J. Wang and H. Tian, *Mater. Horizons*, 2013, **1**, 169.
5 J. Boelke and S. Hecht, *Adv. Opt. Mater.*, 2019, 1900404.
6 H. Nie, J. L. Self, A. S. Kuenstler, R. C. Hayward and J. Read de Alaniz, *Adv. Opt. Mater.*, 2019, 1900224.
7 V. A. Barachevsky, *J. Photochem. Photobiol. A Chem.*, 2018, **354**, 61–69.
8 J. Li, H. K. Bisoyi, S. Lin, J. Guo and Q. Li, *Angew. Chemie*, 2019, **131**, 16198–16202.
9 J. Li, H. K. Bisoyi, J. Tian, J. Guo and Q. Li, *Adv. Mater.*, 2019, **31**, 1807751.
10 S. Lin, H. Sun, J. Qiao, X. Ding and J. Guo, *Adv. Opt. Mater.*, 2020, **8**, 2000107.
11 J. C. Crano and R. J. Guglielmetti, Organic Photochromic and Thermochromic Compounds: Volume 2: *Physicochemical Studies, Biological Applications, and Thermochromism*, Plenum Press, New York, 1999th edn., 1999, vol. 2.
12 S. Nigel Corns, S. M. Partington and A. D. Towns, *Color. Technol.*, 2009, **125**, 249–261.
13 H. Tian and J. Zhang, Ed., in *Photochromic Materials: Preparation, Properties and Applications*, Wiley-VCH, First Edit., 2016, pp. 393–415.
14 G. Favaro, F. Ortica, A. Romani and P. Smimmo, *J. Photochem. Photobiol. A Chem.*, 2008, **196**, 190–196.
15 G. Favaro, F. Masetti, U. Mazzucato, G. Ottavi, P. Allegrini and V. Malatesta, *J. Chem. Soc. Faraday Trans.*, 1994, **90**, 333–338.
16 Y. Ma, Y. Yu, P. She, J. Lu, S. Liu, W. Huang and Q. Zhao, *Sci. Adv.*, 2020, **6**, DOI: 10.1126/sciadv.aaz2386.
17 A. Gonzalez, E. S. Kengmana, M. V. Fonseca and G. G. D. Han, *Mater. Today Adv.*, 2020, **6**, 100058.
18 R. Pardo, M. Zayat and D. Levy, *Chem. Soc. Rev.*, 2011, **40**, 672–87.
19 H. Torres-Pierna, C. Roscini, A. Vlasceanu, S. L. Broman, M. Jevric, M. Cacciarini and M. B. Nielsen, *Dye. Pigment.*, 2017, **145**, 359–364.
20 N. Vázquez-Mera, C. Roscini, J. Hernando and D. Ruiz-Molina, *Adv. Opt. Mater.*, 2013, **1**, 631–636.
21 Y. Kishimoto and J. Abe, *J. Am. Chem. Soc.*, 2009, **131**, 4227–4229.
22 A. Kimoto, A. Tokita, T. Horino, T. Oshima and J. Abe, *Macromolecules*, 2010, **43**, 3764–3769.
23 N. Ishii and J. Abe, *Appl. Phys. Lett.*, 2013, **102**, 163301.
24 T. Yamaguchi, Y. Kobayashi and J. Abe, *J. Am. Chem. Soc.*, 2016, **138**, 906–913.
25 Y. Kobayashi, K. Mutoh and J. Abe, *J. Phys. Chem. Lett.*, 2016, **7**, 3666–3675.
26 Y. Kobayashi, K. Shima, K. Mutoh and J. Abe, *J. Phys. Chem. Lett.*, 2016, **7**, 3067–3072.
27 Y. Kobayashi, Y. Mishima, K. Mutoh and J. Abe, *Chem. Commun.*, 2017, **53**, 4315–4318.
28 A. Tokunaga, K. Mutoh, T. Hasegawa and J. Abe, *J. Phys. Chem. Lett.*, 2018, **9**, 1833–1837.
29 K. Mutoh, M. Sliwa, E. Fron, J. Hofkens and J. Abe, *J. Mater. Chem. C*, 2018, **6**, 9523–9531.
30 S. Toshimitsu, K. Shima, K. Mutoh, Y. Kobayashi and J. Abe, *ChemPhotoChem*, 2019, **3**, 487–494.
31 K. Yamamoto, K. Mutoh and J. Abe, *J. Phys. Chem. A*, 2019, **123**, 1945–1952.
32 A. Kometani, Y. Inagaki, K. Mutoh and J. Abe, *J. Am. Chem. Soc.*, 2020, DOI:10.1021/jacs.0c02455.
33 R. Usui, K. Yamamoto, H. Okajima, A. Sakamoto, J. Abe and Y. Kobayashi, *J. Am. Chem. Soc.*, 2020, DOI:10.1021/jacs.0c02739.
34 H. Kuroiwa, Y. Inagaki, K. Mutoh and J. Abe, *Adv. Mater.*, 2019, **31**, 1805661.
35 Y. Inagaki, Y. Kobayashi, K. Mutoh and J. Abe, *J. Am. Chem. Soc.*, 2017, **139**, 13429–13441.
36 C. M. Sousa, J. Berthet, S. Delbaere and P. J. Coelho, *Dye. Pigment.*, 2019, **169**, 118–124.

37 C. M. Sousa, J. Berthet, S. Delbaere, A. Polónia and P. J. Coelho, *J. Org. Chem.*, 2015, **80**, 12177–12181.
38 C. M. Sousa, J. Berthet, S. Delbaere and P. J. Coelho, *J. Org. Chem.*, 2012, **77**, 3959–3968.
39 C. M. Sousa, J. Berthet, S. Delbaere, A. Polónia and P. J. Coelho, *J. Org. Chem.*, 2017, **82**, 12028–12037.
40 C. M. Sousa, J. Pina, J. S. De Melo, J. Berthet, S. Delbaere and P. J. Coelho, *Org. Lett.*, 2011, **13**, 4040–4043.
41 P. Barbosa, C. M. Sousa and P. J. Coelho, *J. Photochem. Photobiol. A Chem.*, 2020, **388**, 112155.
42 C. M. Sousa and P. J. Coelho, *European J. Org. Chem.*, 2020, 985–992.
43 B. Li, Z. Sun, Y. Zhai, J. Jiang, Y. Huang and J. Meng, *Tetrahedron*, 2019, 130471.
44 M. Tomasulo, S. Sortino and F. M. Raymo, *Adv. Mater.*, 2008, **20**, 832–835.
45 M. Tomasulo, S. Sortino, A. J. P. White and F. M. Raymo, *J. Org. Chem.*, 2005, **70**, 8180–8189.
46 T. Gushiken, M. Saito, T. Ubukata and Y. Yokoyama, *Photochem. Photobiol. Sci.*, 2010, **9**, 162–171.
47 N. Malic, I. J. Dagley and R. A. Evans, *Dye. Pigment.*, 2013, **97**, 162–167.
48 F. Ercole, N. Malic, T. P. Davis and R. A. Evans, *J. Mater. Chem.*, 2009, **19**, 5612–5623.
49 R. A. Evans, T. P. Davis, L. H. Yee, D. A. Lewis, T. L. Hanley, G. K. Such, M. A. Skidmore and G. E. Ball, *Nat. Mater.*, 2005, **4**, 249–253.
50 N. Malic, J. A. Campbell, A. S. Ali, C. L. Francis and R. A. Evans, *J. Polym. Sci. Part A Polym. Chem.*, 2011, **49**, 476–486.
51 W. Sriprom, M. Néel, C. D. Gabbutt, B. M. Heron and S. Perrier, *J. Mater. Chem.*, 2007, **17**, 1885–1893.
52 C. Peterson and M. A. Hillmyer, *ACS Appl. Polym. Mater.*, 2019, **1**, 2778–2786.
53 B. Schaudel, C. Guermeur, C. Sanchez, K. Nakatani and J. A. Delaire, *J. Mater. Chem.*, 1997, **7**, 61–65.
54 D. Levy, *Chem. Mater.*, 1997, **9**, 2666–2670.
55 J. Allouche, A. Le Beulze, J.-C. Dupin, J.-B. Ledeuil, S. Blanc and D. Gonbeau, *J. Mater. Chem.*, 2010, **20**, 9370–9378.
56 Agency for science, technology and research, US Pat. 20120309761, 2012.
57 S. Long, S. Bi, Y. Liao, Z. Xue and X. Xie, *Macromol. Rapid Commun.*, 2014, **35**, 741–746.
58 B. G. Wirnsberger, B. J. Scott, B. F. Chmelka and G. D. Stucky, *Adv. Mater.*, 2000, **12**, 1450–1454.
59 F. Ribot, A. Lafuma, C. Eychenne-Baron and C. Sanchez, *Adv. Mater.*, 2002, **14**, 1496–1499.
60 L. A. Mühlstein, J. Sauer and T. Bein, *Adv. Funct. Mater.*, 2009, **19**, 2027–2037.
61 L. Raboin, M. Matheron, J. Biteau, T. Gacoin and J.-P. Boilot, *J. Mater. Chem.*, 2008, **18**, 3242–3248.
62 N. Andersson, P. Alberius, J. Örtegren, M. Lindgren and L. Bergström, *J. Mater. Chem.*, 2005, **15**, 3507–3513.
63 D. E. Williams, C. R. Martin, E. A. Dolgopolova, A. Swifton, D. C. Godfrey, O. A. Ejegbavwo, P. J. Pellechia, M. D. Smith and N. B. Shustova, *J. Am. Chem. Soc.*, 2018, **140**, 7611–7622.
64 H. A. Schwartz, S. Olthof, D. Schaniel, K. Meerholz and U. Ruschewitz, *Inorg. Chem.*, 2017, **56**, 13100–13110.
65 D. Samanta, D. Galaktionova, J. Gemen, L. J. W. Shimon, Y. Diskin-Posner, L. Avram, P. Král and R. Klajn, *Nat. Commun.*, 2018, **9**, 641.
66 D. Samanta, J. Gemen, Z. Chu, Y. Diskin-Posner, L. J. W. Shimon and R. Klajn, *Proc. Natl. Acad. Sci.*, 2018, **115**, 9379–9384.
67 A. M. Sanchez and R. H. De Rossi, *J. Org. Chem.*, 1996, **61**, 3446–3451.
68 A. Julià-López, J. Hernando, D. Ruiz-Molina, P. González-Monje, J. Sedó and C. Roscini, *Angew. Chemie - Int. Ed.*, 2016, **55**, 15044–15048.
69 A. Julià-López, D. Ruiz-Molina, J. Hernando and C. Roscini, *ACS Appl. Mater. Interfaces*, 2019, **11**, 11884–11892.
70 N. A. Vázquez-Mera, C. Roscini, J. Hernando and D. Ruiz-Molina, *Adv. Funct. Mater.*, 2015, **25**, 4129–4134.
71 N. A. Vázquez-Mera, J. R. Otaegui, R. S. Sánchez, G. Prats, G. Guirado, D. Ruiz-Molina, C. Roscini and J. Hernando, *ACS Appl. Mater. Interfaces*, 2019, **11**, 17751–17758.
72 Y. Tsuru, M. Kohri, T. Taniguchi, K. Kishikawa, T. Karatsu and M. Hayashi, *J. Colloid Interface Sci.*, 2019, **547**, 318–329.
73 E Ink Corporation, US Pat., 7848007B2, 2010.
74 A. Morales, M. Á. Andrés, J. Labidi and P. Gullón, *Ind. Crops Prod.*, 2019, **131**, 281–292.
75 P. S. Drzaic, *J. Appl. Phys.*, 1986, **60**, 2142–2148.
76 Appleton Papers Inc., US Pat., 8440265B2, 2013.
77 L. L. Beecroft and C. K. Ober, *Chem. Mater.*, 1997, **9**, 1302–1317.
78 C. Rovera, M. Ghaani and S. Farris, *Trends Food Sci. Technol.*, 2020, **97**, 210–220.
79 K. S. Miller and J. M. Krochta, *Trends Food Sci. Technol.*, 1997, **8**, 228–237.
80 J. W. Gentry, *J. Aerosol Sci.*, 1997, **28**, 1365–1372.
81 C. Coco, Caprylis Oil (FCO) Safety Data Sheet, Coop Coco, (2017). https://coopcoco.ca/en/oil/caprylis-oil-FCO (last access June 28th, 2020).
82 D. Wong and J. Parasrampuria, *Anal. Profiles Drug Subst. Excipients*, 1996, **24**, 397–441.
83 T. Feczkó, M. Kovács and B. Voncina, *J. Photochem. Photobiol. A Chem.*, 2012, **247**, 1–7.
84 C. Salemi-Delvaux, M. Campredon, G. Giusti and R. Guglielmetti, *Mol. Cryst. Liq. Cryst. Sci. Technol. Sect. A Mol. Cryst. Liq. Cryst.*, 1997, **297**–**298**, 61–68.
85 G. Baillet, Mol. Cryst. Liq. Cryst. Sci. Technol. Sect. A Mol. Cryst. Liq. Cryst., 1997, **297**–**298**, 75–82.
86 Y. Xiong, A. Vargas Jentzsch, J. W. M. Osterrieth, E. Sezgin, I. V. Sazanovich, K. Reglinski, S. Galiani, A. W. Parker, C. Eggeling and H. L. Anderson, *Chem. Sci.*, 2018, **9**, 3029–3040.
87 K. M. Louis, T. Kahan, D. Morley, N. Peti and R. S. Murphy, *J. Photochem. Photobiol. A Chem.*, 2007, **189**, 224–231.
88 A. Kellmann, F. Tfibel, R. Dubest, P. Levoir, J. Aubard, E. Pottier and R. Guglielmetti, *J. Photochem. Photobiol. A Chem.*, 1989, **49**, 63–73.